Pal *et al. Journal of Translational Medicine* (2025) 23:577
https://doi.org/10.1186/s12967-025-06593-1

Journal of Translational Medicine

RESEARCH Open Access

Patient-derived esophageal adenocarcinoma organ chip: a physiologically relevant platform for functional precision oncology

Sanjima Pal[1], Elee Shimshoni[2], Salvador Flores Torres[3], Mingyang Kong[4], Kulsum Tai[4], Veena Sangwan[1,4], Nicholas Bertos[1], Swneke Donovan Bailey[1,4], Julie Bérubé[1], Donald E. Ingber[2†] and Lorenzo Ferri[1,4*†]

Abstract

Background Esophageal adenocarcinoma (EAC) is the sixth most deadly cancer worldwide, with increasing incidence in North America. As no targeted therapy or immunotherapy has revolutionized the management of EAC, chemotherapy is the only standard of care. Most patients with EAC experience poor outcomes because of the inherent or acquired resistance to chemotherapy.

Methods Adapting a patient-centered approach, we leveraged a microfluidic cell culture technology platform (Emulate), organoids derived from treatment-naive patient tumors or adjacent normal tissues, and patient-matched cancer-associated or normal fibroblasts respectively, to develop a novel, physiologically relevant, high-fidelity preclinical esophagus-on-a-chip model. H&E, immunofluorescence staining, live/dead assay, LDH assay, and ELISA-based detection of tumor biomarkers were used to assess treatment responses.

Results Each patient-specific stroma-inclusive microfluidic esophageal adenocarcinoma on-a-chip (EAC chip) faithfully recreates the tumor-stroma interface while preserving the full diversity of two cell types (epithelia and fibroblasts), genetic landscapes and histological architecture of the source tumors. EAC chips also accurately predict the response to neoadjuvant chemotherapy (NACT) within a clinically useful timeframe (approx. 12 days). A docetaxel-based triplet chemotherapy regimen matched with the treatment of the source patient was successfully perfused through the interstitial space within this model. Therefore, EAC chips more accurately recapitulate inpatient pathological and objective responses than the corresponding static 3D-organoid-only cultures.

Conclusions Overall, this model is an effective tool for predicting patients' responses to chemotherapy and testing tumor- or stroma-targeted alternative therapies. Moreover, these high-fidelity, low-throughput EAC chips effectively complement high-throughput PDO culture-based drug testing and provide improved insights into drug efficacy before human studies.

†Donald E. Ingber and Lorenzo Ferri contributed equally to this work.

*Correspondence:
Lorenzo Ferri
lorenzo.ferri@mcgill.ca

Full list of author information is available at the end of the article

Graphical Abstract

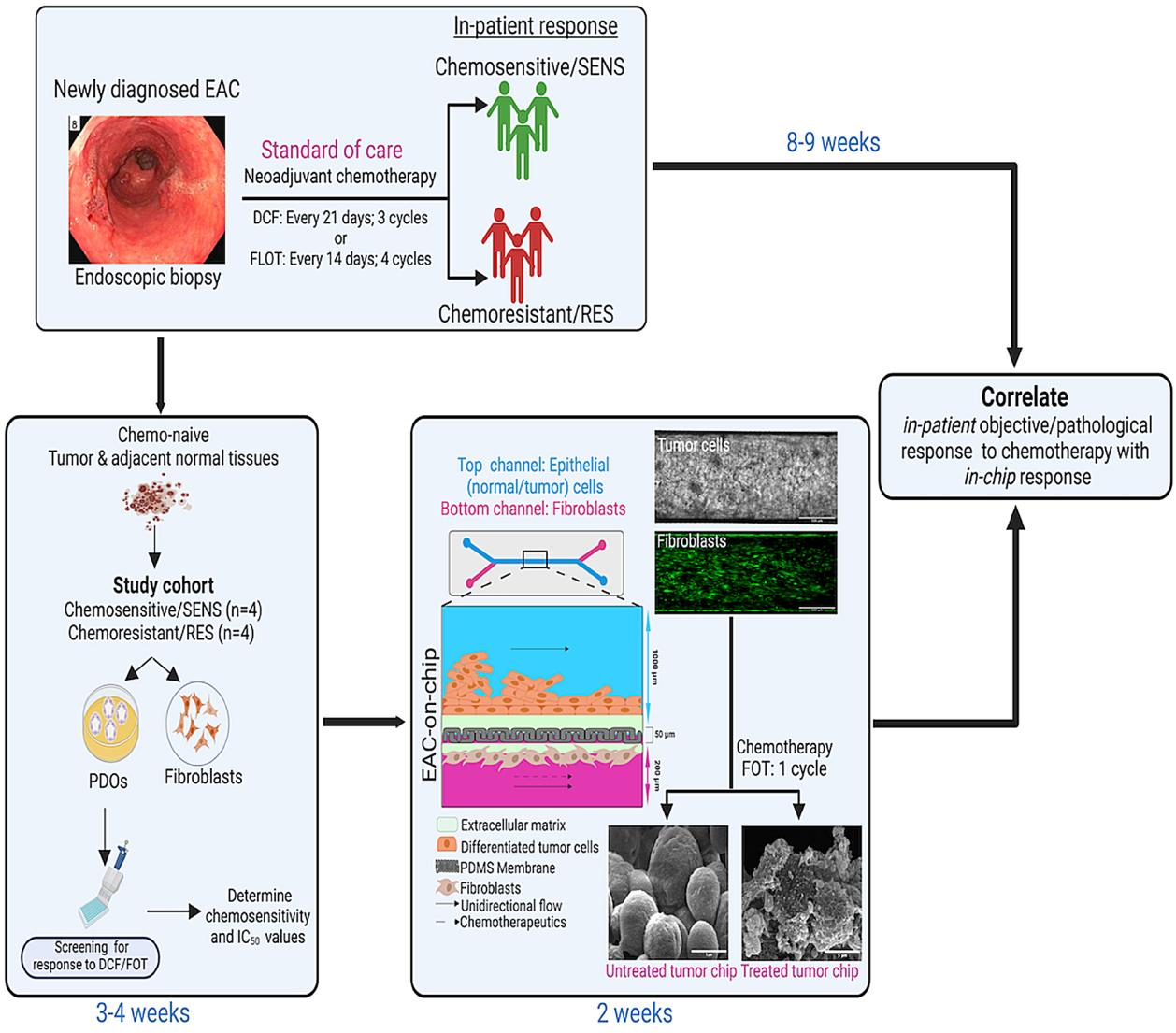

Keywords Esophageal adenocarcinoma, Organ-on-a-chip, Organoids, Cancer-associated fibroblasts

Introduction

EAC tumors exhibit ab initio chemotherapy resistance. Meanwhile, most responders to neoadjuvant chemotherapy (NACT) exhibit high rates of progression and metastasis during the adjuvant period. Given the lack of alternative approaches, each non-responder to NACT continues to receive the SOC as adjuvant therapy. The development of accurate.

Esophageal adenocarcinoma (EAC) is the fastest-rising malignancy in North America [1]. The only standard-of-care (SOC) treatment for locally advanced, resectable EAC is perioperative docetaxel-based triplet chemotherapy (Table S1) [2]. Most EAC tumors exhibit ab initio chemotherapy resistance. Meanwhile, most responders to neoadjuvant chemotherapy (NACT) exhibit high rates of progression and metastasis during the adjuvant period. Given the lack of alternative approaches, each non-responder to NACT continues to receive the SOC as adjuvant therapy. The development of accurate and in vivo preclinical models, prognostic markers for response to therapy, and alternative effective treatments for chemoresistant EAC patients all remain critical unmet clinical needs.

Patient-derived organoid (PDO) culture recapitulates the heterogeneity of epithelial cell lineages more faithfully than traditional 2-dimentional (2D) cell lines do

[3–6]. These cancer organoids have been effectively used for high-throughput (HTP) screening of monotherapies and for predicting patient outcomes [7–11]. There are also reports highlighting the ineffectiveness of PDOs in predicting the outcome of treatment with 5-fluorouracil (5-FU) combined with oxaliplatin [12].

Traditionally, organoids grow in complex 3-dimentional (3D)-Matrigel domes, and cultures are maintained under static conditions. Matrigel, a heterogeneous mixture of murine sarcoma-derived ECM proteins, exhibits lot-to-lot varying concentration, stiffness and influences drug diffusion [13]. Thus, PDO culture format often suffers from poor reproducibility [14]. To address this critical issue, several groups have used well-defined micro-engineered hydrogels or alginates as alternatives to Matrigel, especially for incorporating user-defined microenvironmental signals to investigate human epithelial tumors [15–18]. Thus the in vitro response of PDOs may diverge from the observed response in patients, especially for combination therapy where each drug may have a distinct pharmacokinetic profile and toxicity (e.g. docetaxel).

Since organoids lack various cellular (stromal and immune) and physiological factors (oncotic pressure and interstitial fluid movement) of the tumor microenvironment (TME), they often fail to fully capture the intricacies of drug efficacy and distribution observed in actual tumors [18–23]. There is thus significant room to improve on cancer organoid technology by combining organoids and stromal cells to develop a higher-fidelity platform that more effectively recapitulates human-relevant esophageal organ structure, cellular/tissue heterogeneity, physiology, pathogenesis, and drug distribution and is more likely to accurately predict in patient response to therapy [8].

Although still a low-throughput system, microfluidic organ-chip technology offers multiple advanced features that are lacking in static organoid culture technology, including recapitulation of the organ-level TME [24–26]. Organ Chips provide dynamic fluid flow and thus provide a unique opportunity to mimic human relevant pharmacokinetic and pharmacodynamic (PK/PD) profiles of drugs in vitro to recapitulate treatment regimen-specific drug efficacy and toxicity [27–32]. Additionally, organ chips also demonstrated some translatable endpoints similar to those observed for human pathophysiology [28, 33].

Here, we highlight a key limitation of 3D PDO culture technology and propose an improved approach by integrating PDO and cancer-associated fibroblast (CAF) co-cultures with microfluidic organ-on-a-chip technology. We describe a first-generation, syngeneic human EAC-Chip platform containing PDO-derived EAC cells separated by a porous membrane from patient-matched CAFs, co-cultured under continuous flows of nutrient media. Furthermore, we also demonstrate that the EAC-chip platform achieves clinical mimicry when a triplet chemotherapy regimen is perfused through the bottom (stromal) channel lined with CAFs.

Methods

Study cohort

Consented patients with locally advanced resectable EAC ($n=8$) who received triplet NACT were selected for the current study (Fig. 1B). Patients were divided into two groups, **(i) Chemosensitive (SENS)** ($n=4$) patients who demonstrated either complete or partial objective response (OR) to NACT. **(ii) Chemoresistant (RES)** ($n=4$) patients were either clinically assessed for stable disease (SD) or progressive disease (PD) following NACT.

Isolation and propagation of a syngeneic patient-derived epithelial/tumor niche and associated fibroblasts

Tissue specimens were collected from the adenocarcinoma and adjacent normal regions at the time of diagnostic endoscopic biopsy. Organoids and regional fibroblasts were established from the specimens and propagated using the protocol below.

Briefly, the tissue was minced and enzymatically digested with tissue digestion buffer in a GentleMACS-STM Octo Dissociator with heaters (Milltenyi Biotec.). The cell pellets were obtained and trypsinized to obtain single cells. The resulting cells were resuspended and were allowed to stand undisturbed for 10 min. Later a fraction was transferred to a new tube for fibroblast culture and centrifuged.

For fibroblast propagation

Cell pellets were resuspended in 1 ml fibroblast propagation medium and seeded in Type I collagen precoated plates.

For organoid propagation

Cell pellet was resuspended in ice cold Matrigel and plated. Organoids in Matrigel domes were maintained in *expansion medium*. Mature PDOs were passaged after 10–12 days. Single cells were obtained through enzymatic digestion and trypsinization.

Both PDOs and associated fibroblasts were cultured under hypoxic conditions, i.e., 3% O_2. All consumables used for each method are listed in Table S4.

For analysis of organoid histology, Histogel blocks were prepared following an existing protocol (https://ccr.cancer.gov/sites/default/files/2022-11/Histogel_Protocol_0.pdf).

Culture of stroma-exclusive, fragmented and dispersed PDOs under static conditions

Fragmentated PDOs were obtained with TrypLE™ (Invitrogen 12605010) at 37 °C for 1 min. 5000 fragmented

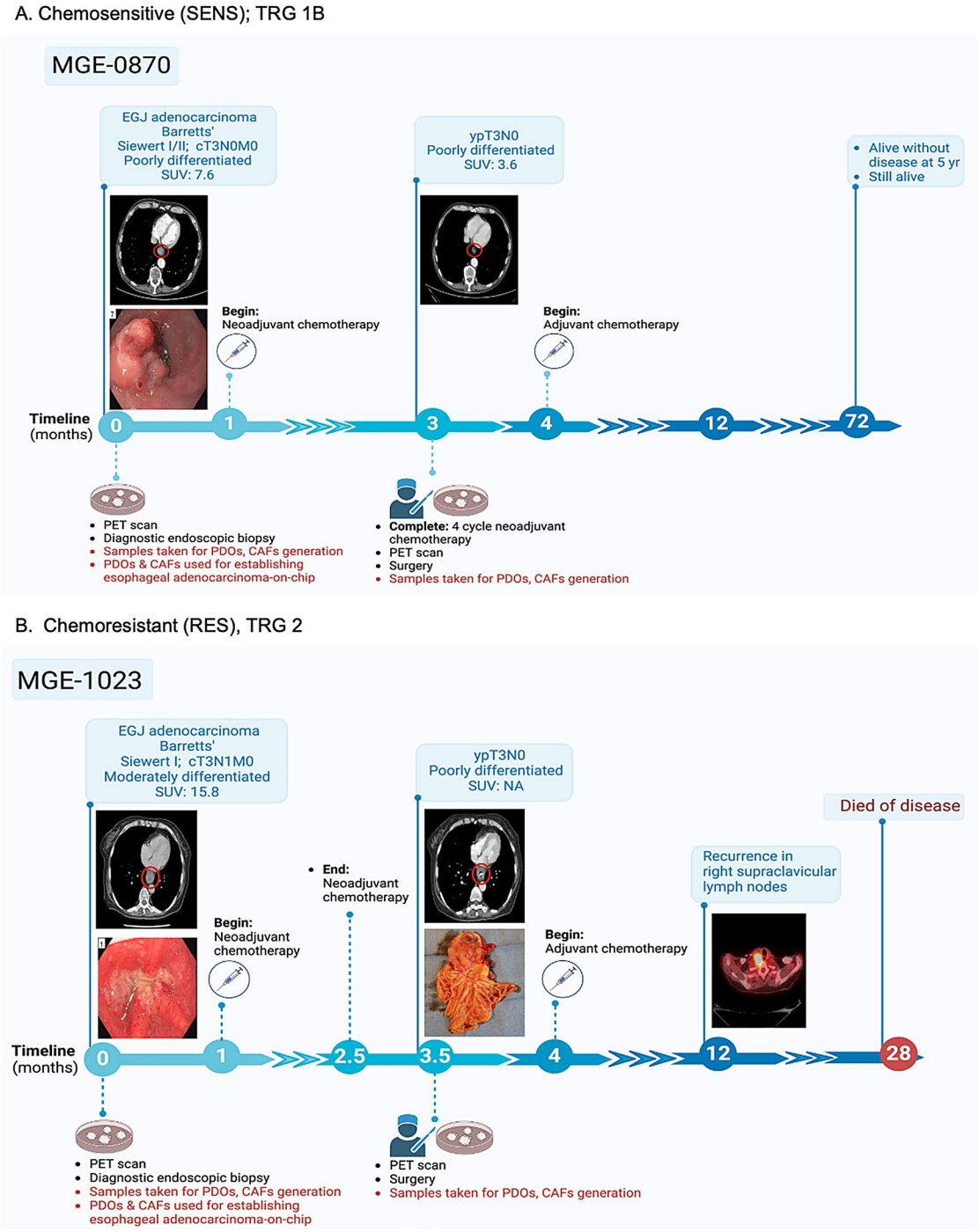

Fig. 1 Patient treatment timeline. Timelines of diagnosis, treatment, response to treatment, and PDO generation in representative **(A)** chemosensitive (SEN) and **(B)** chemoresistant (RES) patients

PDOs were seeded on ECM precoated 96 well plates and maintained in organoid expansion medium. On the sixth day post-seeding, the *expansion medium* (EM) was replaced with *differentiation medium (DM)* which was maintained throughout the experiment. Cells were maintained for 12 days and harvested for measuring cell viability and microscopy.

Establishment of syngeneic esophageal tissue-on-a-chip

The complete organ-on-a-chip setup (Chip-S1™ stretchable organ chips, POD™ portable modules, Zoe-CM-1™ culture module and Orb-HM1™ Hub Module) was procured from Emulate Inc. The chip design comprises two parallel microfluidic channels, separated by an optically transparent 50 µm PDMS porous membrane (7 µm

diameter). On day 0, chip surfaces were activated with S1 chip activation solution and high-power UV light. The activated membrane was coated with freshly prepared ice-cold ECM solution (ST4) and incubated overnight. On day 1, PDO-derived fragmented organoids or epithelial cells (concentration: 3×10^6 cells /ml) were seeded at the upper channel. Once cells adhered to the membrane (~4 h), the chips were connected to flow at 60 µl/h. Patient matched regional fibroblasts were seeded in the lower stromal channel of the chip on day 2. Fibroblasts were incubated for 4 h at 37 °C before chips were reconnected to flow at 60 µl/h. On day 6 post-seeding of epithelial cells, the expansion media in the epithelial inlets were replaced with differentiation media. Overall chips were maintained up to 12 days. The development of PDOs and microtissues (day 0 to day 12), morphological changes and the population of cells undergoing treatment-induced cell death were also determined by brightfield and fluorescence microscopy respectively (EVOS, Invitrogen).

Detailed protocol (Standard operating protocol) has been supplied as Document S1.

Histological analysis of primary and chip derived microtissues organ chips

Primary tissue samples fixed in 10% formalin were dehydrated with alcohol and then embedded in paraffin. 5 µm thick sections were prepared, mounted on glass slides, stained with H&E and analyzed. On Day 13, Tissue-Tek® OCT compound (Thermo Fisher Scientific) was administered through both channels of 4% PFA fixed microtissues and OCT-blocks were created. 30 µm vertical cross-sections were prepared, stained with H&E and imaged (EVOS M7000).

Whole-exome sequencing and analysis

PDOs were passaged for at least 5 generations to collect ample amount of genomic DNA and develop EAC-chips. H&E-stained tissue sections were reviewed by an expert pathologist before isolation of the DNA. A primary tissue sample with tumor content ≥ 50% was submitted for WES. Genomic DNA was extracted (Qiagen: Cat. No.80204) from snap frozen primary tissue, matched organoids, and chip derived cells from upper epithelial channel. DNA extracted from blood (buffy coat) was used as a germline reference.

To compare the genomic similarities between the primary tumor biopsy, organoid and organ-on-chip samples, we aligned the WES reads to the human reference genome (GRCh38) using the Burrows-Wheeler Aligner (BWA) [34]. Duplicate reads were marked and base quality scores were recalibrated using the genome analysis toolkit (GATK) [35]. Somatic mutations were called for the primary tumour, organoid and organ-on-chip against a patient matched normal sample using muTect [36]. Somatic mutations were annotated with ANNOVAR [37]. Acquired copy number alterations (CNA), including regions of loss of heterozygosity (LOH), were determined using FACETS [38]. The mutation allele frequencies were determined with bam-readcount [39].

Immunofluorescence microscopy studies

12-day old chips were fixed with 4% PFA and cut into 300 µm vertical cross sections using a vibratome (Leica VT1200). Immunofluorescence staining was carried out using manufacturer's suggested dilutions of the primary, secondary antibodies and DAPI nuclear stain (Table S4). Stained chip sections were imaged using a Zeiss LSM 780 confocal microscope. Whole-mount 3D-PDO culture immunofluorescence was performed *via* a 3D tissue clearing kit (5730, Corning) according to the manufacturer's protocol. Images of organoid were captured using either in EVOS M7000 and ZEISS Lattice SIM 3.

Scanning electron microscopy (SEM)

Both treated and untreated EAC-chips were fixed with 4% PFA solution and washed 3 times with PBS. Concomitantly, the chip was trimmed using a razor blade, and 300 µm vertical cross sections were prepared using vibratome. Afterward, the samples were gradually dehydrated in 100% ethanol and placed in a critical point dryer (CPD030, Leica) and 20 × 1-minute CO_2 exchange cycles were performed. Samples were sputter-coated (ACE600, Leica) with an 8 nm layer of platinum. images were acquired using an Environmental Scanning Electron Microscope (Quanta 450, FEI).

Assessment of apparent permeability

The degree of epithelial barrier integrity was determined following an existing protocol (https://emulatebio.com/wp-content/uploads/2021/06/EP187_v1.0_Barrier_Function_Analysis_Protocol.pdf). Data were obtained from 10 chips derived from 3 source patients (2–4 chips/donor).

Assessment of intrinsic response of intact PDOs to neoadjuvant therapy under static conditions

PDOs were enzymatically dissociated and 10,000 cells per 30 ul of Matrigel/well were distributed in a 96-well plate. 200 ul of OEM was dispensed into each well. In vitro drug treatments were conducted in triplicate at concentrations ranging from 0 to 1 µM of F: C:T docetaxel with ratio of 10:1:1 respectively. Triplicate chemotherapeutics at relevant doses (described in Table S2) were added together for 72 h. Solvent percentage was limited to 0.1%. As Matrigel is soft and does not adhere tightly to the surface, replacing the media with or without triplet chemotherapeutics in a 96-well format was technically unfeasible. The percent viability of intact PDOs was

measured after 72 h of treatment using the CellTiter-Glo 3D reagent (Promega, G9681) according to the manufacturer's instructions. Luminescence was measured via Varioskan LUX Multimode Microplate Reader (Thermo Scientific). The experimental readings were normalized to respective solvent controls. Viability curves and IC_{50} values were generated using GraphPad Prism 8 software.

Clinically relevant drug dosing for static and dynamic culture conditions

The actual FLOT regimen and clinically relevant dosing reconstituted for the microfluidic culture is described in Table S2. Leucovorin was omitted, since it is not a chemotherapeutic agent. Fragmented and dispersed PDOs were seeded in ECM solution coated 96 well plates. Cells were directly exposed to one cycle of FOT on day 8 (Table S2). Cellular viability was determined on day 12 as described above. The data are representative of biological and technical triplicates.

EAC-Chips achieved human relevant epithelial tissue integrity within 5 days under dynamic conditions and treatment began on day 8. FOT chemotherapy was administered through the stromal channel. At first, a flush cycle (< Cmax, FOT: 52:1.7:1] of 1–2 min with a flow rate of 1000 µl/h in the bottom channel and 0 µl/h top channel was performed to ensure proper distribution of the drugs only in the stromal microfluidic channel networks. To mimic bolus IV-injection, during the first hour of cycle a mixture of all three chemotherapeutics was administered at a flow rate of 100 µl/h, followed by only a mixture of oxaliplatin (O) and 5FU (F) at the rate 60 µl/h for another hour. Only 5FU (F) was subsequently perfused through the stromal channel at a flow rate of 60 µl/h for a total of 24 h.

Measurement of LDH activity

On day 9, effluents from epithelial channels were collected and samples were immediately assayed for LDH activity using the Promega™ LDH Cytotoxicity Assay Kit (Promega #G1781). All absorbance-related measurements were performed in a Varioskan LUX Multimode Microplate Reader (Thermo Scientific). The resulting data are shown as percentage of cell cytotoxicity. Two-way ANOVA was used to assess differences in the cell-free LDH activity in the effluents from treated and untreated groups.

Propidium iodide (PI) assay

On day 12, media was aspirated from the inlet reservoir of the epithelial channel and replaced with fresh culture medium supplemented with PI (Sigma #P4170) for 5 min. The samples were subsequently washed with PBS. Images of 5–6 random regions of each chip were captured using a EVOS microscope. The non-parametric Mann-Whitney U-Wilcoxon test was employed to compare number of dead cells (defined as having an average cell area ≥ 100 µm²) in both treated as well as untreated SENS and RES samples.

Measurement of tumor-derived extracellular soluble fragments of CK19

On day 11, effluents were collected from outlet reservoirs of epithelial channels of both treatment naïve and FLOT treated chips. Chemo-naïve sera were collected ($n = 10$) at the time of diagnostic endoscopy. Soluble CK19 fragment concentration in serum and effluents were measured using ELISA (Elabscience®, E-EL-H2077) as per the manufacturer's instructions. The data analyzed are displayed as a percentage of reduction in the soluble CK19 fragments in treated effluents compared with untreated chips.

Statistical analysis

GraphPad Prism 8 software (www.graphpad.com) was used for statistical analysis. *p value* < 0.05 was considered as significant for each analysis. *<0.05; **<0.01, ***<0.005 ***<0.001; ns: not significant.

Results

Schematic representation of the strategy adapted to develop personalized human EAC-chips and clinicopathological characteristics of the study cohort

Our comprehensive strategy for modeling patient-derived esophageal adenocarcinoma chips, utilizing both PDOs and associated fibroblasts from the same patient source, for functional precision oncology were demonstrated as a graphical abstract. Esophageal PDOs and matched fibroblasts were generated from endoscopic biopsies of 8 newly diagnosed, treatment-naïve patients with locally advanced EAC (Table 1). Subsequent pathological (tumor regression grade/TRG) and objective radiographic (RECIST v1.1) responses to docetaxel-based triplet neoadjuvant chemotherapy were extracted from the medical records. Patients were sub-grouped into either **chemosensitive/SENS** (complete [TRG0] or near-complete [TRG1a-b] pathological response) or **chemoresistant/RES** (moderate [TRG2] or poor [TRG3] pathological response). Representative clinical timelines and longitudinal endoscopic/ PET imaging are depicted in Fig. 1.

Static PDO monocultures enable high throughput at the cost of reduced fidelity

Analysis of selected PDOs (MGE #1181; #0985, #1033, #0099, #1159, #1023) from the EAC patient study cohort revealed that these organoids histologically resemble their primary tissues of origin and maintain cellular complexity, e.g. cohesive morphology (Fig. 2Ai-ii). Tumor tissue-derived 3D PDOs express various epithelial markers,

Table 1 Clinicopathological characteristics of the study cohort. The study cohort was subdivided into chemosensitive and chemoresistant cohorts based on pathological and clinical response to NACT. Patients were HER2-negative and microsatellite stable. All patients except the underlined patients received FLOT. Those patients received DCF. AC: adenocarcinoma; EGJ: esophageal-gastric junction (Siewert II); F: 5-fluorouracil; L: leucovorin; O: Oxaliplatin; T or D: docetaxel; C: cisplatin; objective response: RECIST: response evaluation criteria in solid tumors; PET-SUV response - CR: complete response; PR: partial response; SD: stable disease. GX: undetermined grade. MGE: MUHC-Gastroesophageal. Organoids and corresponding CAFs were collected from the group of patients with locally advanced, resectable EAC before undergoing NACT and were utilized to create EAC chips. Patient specimens, except for the underlined ones, were used to evaluate chemotherapy response on EAC chips

		Patient #	Location of tumor	Grade	Clinical stage	Pathological stage	Pathological response	Objective response
Chemosensitive (SENS)	1	MGE-1181	EGJ	Poor	cT3N1	ypT3N2	TRG 1B	PR
	2	MGE-0985	Distal Esophagus	GX	cT3N0	ypT3N0	TRG 1A	PR
	3	MGE-1033	EGJ	Well	cT4N0	ypT2N0	TRG 1B	CR
	4	MGE-0870	EGJ	Poor	cT3N+	ypT3N0	TRG 1B	PR
Chemoresistant (RES)	1	MGE-0099	EGJ	Moderate	cT3N1	ypT3N2	TRG 2	SD
	2	MGE-1159	EGJ	Poor	cT3N1	ypT3N3M1	TRG 3	SD
	3	MGE-1023	EGJ	Poor	cT3N0	ypT3N0	TRG 2	SD
	4	MGE-0692	EGJ	Poor	cT3N3	ypT3N3	TRG 3	SD

including Pan-cytokeratin (PanCK), a marker of differentiating epithelial tumors, and Ki67, a prognostic and predictive tumor marker. Patient-matched cancer-associated fibroblasts (CAFs) express standard pan-CAF markers such as lumican (LUM) and PDGFRβ. Myofibroblast-like CAFs (myCAFs) are expressing αSMA, while inflammatory CAFs (iCAFs) are expressing PDGFRα (Fig. 2Aiii). Collectively, these data validate the lineage-specific identities of the primary cell types. Static monocultures of treatment naïve 3D-organoids were directly exposed to a defined triplet chemotherapy for 72 h. This approach was designed to achieve patient specific chemosensitivity and minimize additional nonspecific toxicity of chemotherapeutic drugs in vitro. When PDOs are used as an in vitro platform, the area under the drug response curve (AUC), which integrates both drug potency and efficacy, is a more robust and accurate parameter for predicting patient response to combination therapy compared to the half-maximal inhibitory concentration (IC_{50}) [12, 40]. We observed enhanced resolution in the survival curves when comparing the responses of chemosensitive and chemoresistant PDOs after 72 h (Fig. 2B), in contrast to 24–48 h (data not shown). We successfully determined subcytotoxic doses (here, IC_{50} values) for only 5 of 6 PDOs with no significant differences in the mean IC_{50} and AUC values between the groups. Mean percentage of survival at some specified doses frequently overlaps, making it difficult to predict patient response. Additionally, one chemosensitive PDO failed to recapitulate in vivo responses (Fig. 2B.i). The data indicate additional higher-fidelity follow-up steps are necessary before accurately predicting patient responses.

To address the issue of technically difficult media changes with 3D-PDOs in Matrigel, we tested dispersed fragmented 2.5D-PDOs cultured on ECM coated 96-well plates. This High throughput or HTP approach allows us to screen sensitivity of tumor cells against FOT regimen using the precise clinical drug exposure conditions (Table S1-S2; 1 cycle FOT). Here, despite multiple rounds of media replacement, the untreated cells continued to adhere tightly to the ECM-coated surfaces of the 96-well plates, differing from the behavior of cells in 3D Matrigel. However, despite this ability to replicate *inpatient* dosing, the survival of chemosensitive organoids was not found to be significantly different from resistant organoids (Fig. 2B.ii), highlighting the need for a more accurate disease modelling platform.

Establishment and characterization of esophageal-organ-on-a-chip system

We leveraged the microfluidic organ-on-chip platform (Emulate Inc.) to create a more relevant, patient specific,

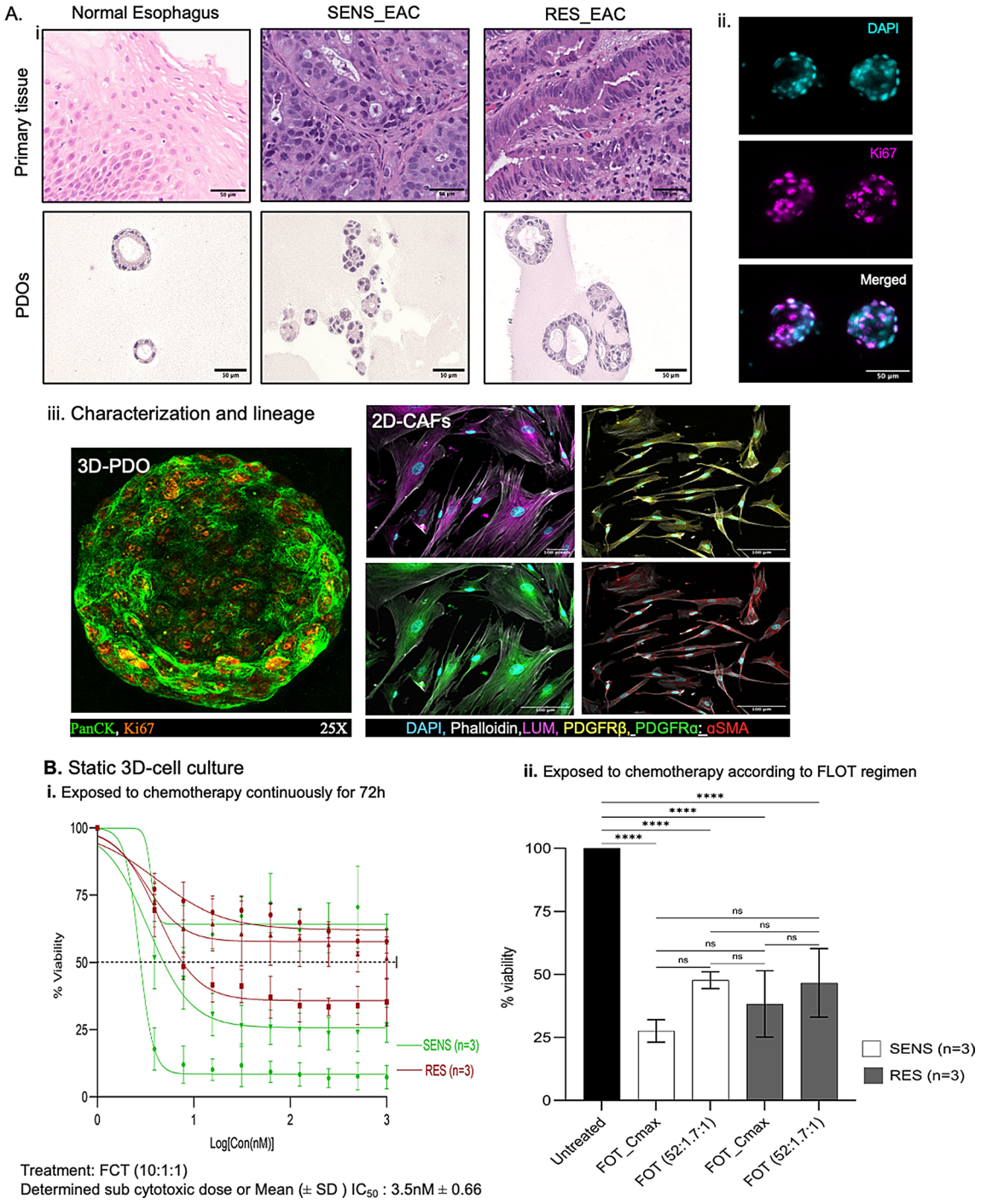

Fig. 2 Static PDO cultures maintained without associated fibroblasts display higher throughput but lower fidelity. **(A) (i)** H&E-stained sections of representative chemonaïve primary tissues and corresponding PDOs. **(ii)** Representative EVOS images of mature EAC tissue-derived PDOs stained with DAPI (cyan) and Ki67 (magenta). 20X objective. Scale bars, 50 mm. **(iii)** PDOs and CAFs were characterized using relevant epithelial and fibroblasts lineage-specific biomarkers. **(B)** Response to treatment measured via the CellTiter-Glo® assay. **(i)** 3D-PDOs were treated with triplet chemotherapy for 72 h, and dose–response curves are displayed. Differences in subcytotoxic IC_{50} doses (determined *via* GraphPad) were not significant between chemosensitive (green; $n = 3$) and chemoresistant (red $n = 3$) PDOs. **(ii)** Fragmented PDOs seeded on ECM-coated wells and exposed to either Cmax or subcytotoxic dose (< Cmax) concentrations of FOT (ST2) on day 8. Viability was determined on day 12. The representative bar graphs (means ± SEMs) show no significant differences in response between the groups

stroma-inclusive, high-fidelity preclinical EAC avatar. The timeline for model development and assessment of treatment response is depicted in Figure S1A. Esophageal PDO derived epithelial cells were grown in the upper "luminal/epithelial" channel, separated by a porous membrane from the lower "vascular/stromal" channel that was lined with patient-matched fibroblasts. When subjected to a physiologically relevant nutrient flow (60 µl/h), the EAC-derived cells proliferate and regenerate at the tumor-stromal interface. Horizontal- and vertical-views of 4% paraformaldehyde (PFA) fixed chips (Fig. 3A) and live microtissues (Fig. 3B) revealed the presence of a characteristic tightly anchored and single-layered squamous epithelium in normal esophagus-chips versus the disorganized and multilayered epithelial cells with glandular protrusions in EAC-chips. A low magnification, cross-sectional image of the chip shows the spatial organization of proliferating epithelial/tumor cells (Ki67$^+$) and CAFs (vimentin$^+$) across the PDMS membrane (Figure S1B). Figure S2 showcases bright-field images of epithelial/tumor side of all 8 chips developed for this study. Each tumor chip exhibits an unpolarized and distinct disorganized arrangement of epithelial/tumor cells, with no evidence of normal, stratified, polarized squamous-like epithelium, further supporting patient specific, heterogeneous tumorigenesis within the chip. SEM analysis of the EAC-chips reveals stacked and closely packed pleiomorphic tumor cells with microvilli (Fig. 3C). The EAC-Chip also displayed a decrease in apparent permeability, indicating the formation of a physiologically relevant tissue barrier, within 5 days (Figure S4A). Interestingly, functional separation between the epithelial and stromal channels of the microfluidic device enables delivery of therapies through the interstitial space (*via* the lower channel) to mimic how cancers are exposed to chemotherapy in vivo.

EAC chips emulate the histology and genetic background of the source patient tissue

Histological analysis of a representative EAC-chip revealed faithful recapitulation of the morphological features of the tumor of origin (Fig. 4A-B and S3). According to findings from TCGA [41], and other research teams [42, 43], copy number alteration (CNA) and loss of heterozygosity (LOH), such as deletions and amplifications, are more common in EAC patients than point mutations. Whole exome sequencing (WES) unraveled a set of shared subclones with mutations in tumor suppressor genes or other oncogenes across source patient tissue, matching the PDO and EAC-chip. Several noteworthy oncogenic driver mutations in tumor suppressor genes such as TP53, SMAD4, KDM6A, and mutations in oncogenes such as LAMA1, ZNF521, CDH2/7, are found to be shared by matched EAC primary tissue, PDO and microtissue on the chip (as shown in Fig. 4B and S5). There are mutations within oncogenes that are exclusively shared by primary tissues and chips e.g. APC, and GATA6.

Evaluation of clinical mimicry in EAC chips

To assess the efficacy of this model for the prediction of treatment efficacy, triplet chemotherapeutic agents were administered *via* the stromal/fibroblast channels of 3 chemosensitive (#1181, #0985, #1033) and 3 chemoresistant (#0099, #1159, #1023) EAC-chips on the 8th day. Figure S1B displays the fibroblast channel through which chemotherapy was administered. Each chip was subjected to one cycle of combination chemotherapy (FOT; >24 h, days 8–9) followed by media flow without chemotherapeutics for 72 h (days 9–12). Confocal microscopic and SEM imaging revealed that the epithelial cells in chemosensitive chips were almost absent from the membrane surface after one cycle of FOT; the few remaining cells displayed an involuted morphology with membrane blebbing and tissue discontinuity (Fig. 5Ai-ii). On the other hand, the chemoresistant cancer-derived epithelial layer remained almost intact, and the cells retained their morphology. Notably, fibroblast layers in the lower channel were maintained after treatment in both cohorts, indicating that the chemotherapy perfused directly through the stroma-lined channel at *inpatient*-equivalent doses selectively kills chemosensitive epithelial cancer cells. In addition, propidium iodide (PI)-based live-dead cell imaging further demonstrated increased cell death following treatment in chemosensitive EAC chips, with greater nuclear incorporation of PI after treatment than in chemoresistant samples (Fig. 5B and S6). LDH release, a measure of plasma membrane damage and cancer cell death, was significantly higher in the effluents of the epithelial channel of chemosensitive EAC-chips than in those of chemoresistant EAC-chips collected immediately following FOT administration (Fig. 5C).

Representative images of the disease-free (normal) esophagus-on-a-chip show intact epithelial layer with insignificant number of dead cells following administration of the same doses of FOT, perfused through the stromal channel (Figure S4C). Interestingly, when the same chemotherapeutic agents were perfused directly into a chemoresistant cancer cells *via* the top channel, significant cytotoxicity was observed and chemoresistant EAC-Chip failed to accurately replicate the *inpatient* response (Figure S4B), confirming that physiologically relevant delivery of these chemotherapeutic agents through the interstitial space (or stromal channel) is a key requirement for mimicking features of the TME and creating a patient-relevant model.

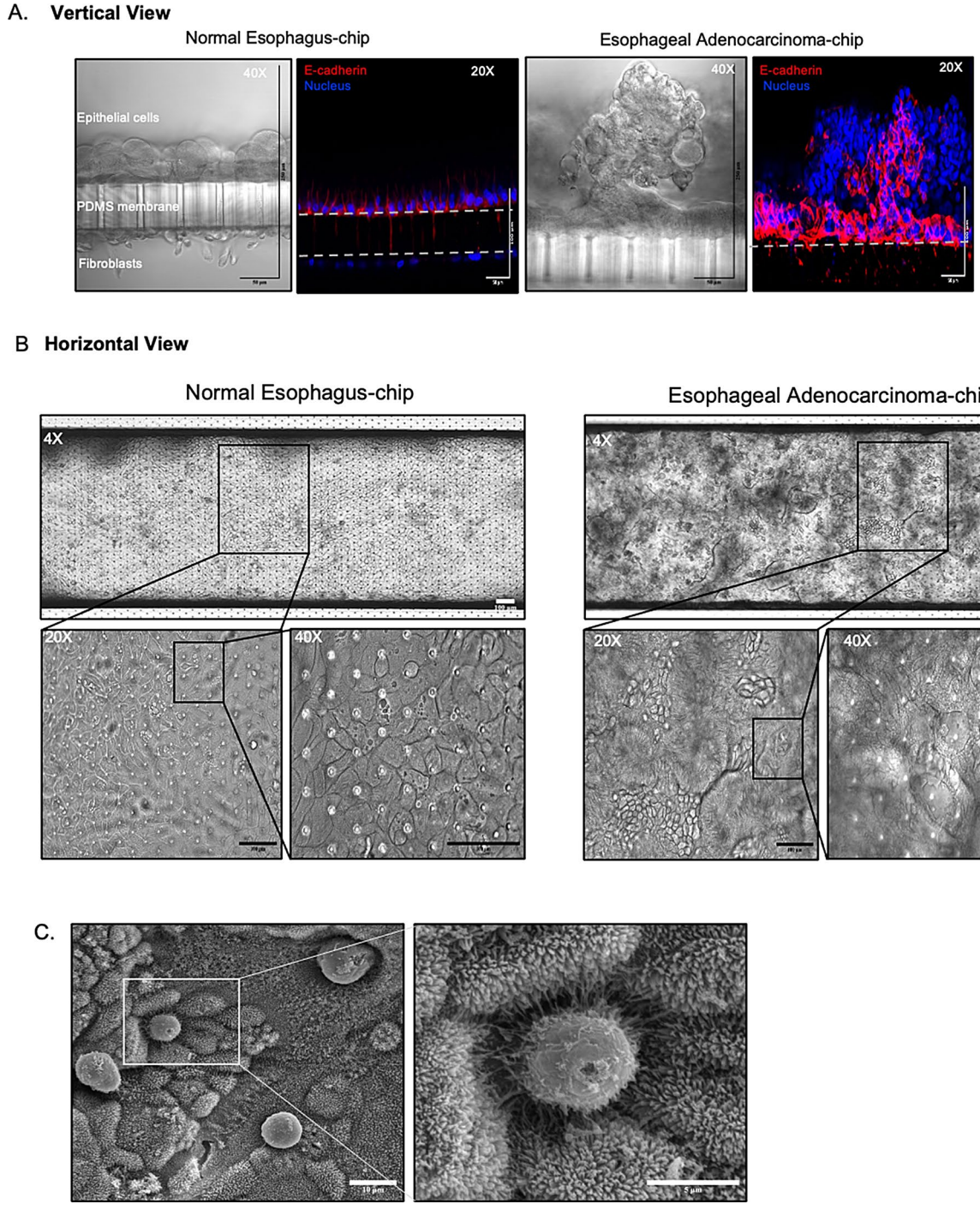

Fig. 3 Establishment and characterization of esophageal organ-on-chip systems. PDO-derived normal or EAC epithelial cells were cultured in the upper "epithelial" channel, along with patient- and tissue-matched fibroblasts in the lower "stromal" channel, for 12 days under continuous flow. **(A)** Brightfield (left) and immunofluorescence (right) images of vertical sections show cell patterns as well as interfaces between the epithelial layer and fibroblasts. The gray dashed lines indicate the boundaries of the porous PDMS membrane. **(B)** Horizontal brightfield images of chip microtissues showing a characteristic squamous epithelium layer (normal esophagus-on-chip) or irregular adenocarcinoma-like glandular formations (EAC chip). **(C)** SEM images of representative vertical cross-sections of epithelial surfaces of the EAC chip

Correlation between clinical response (RECIST v1.1) and effectiveness of NACT reconstituted on EAC-chips

Proliferating tumor cells shed fragments of C-terminus of CK19 (40 KDa) or CYFRA 21 – 1 into the serum, and NACT can effectively lower the levels of this circulating tumor marker [44–49]. We measured soluble CK19 fragments in serum of chemo-naïve EAC patients ($n = 10$) (Table S3 and Figure S7) and chip derived

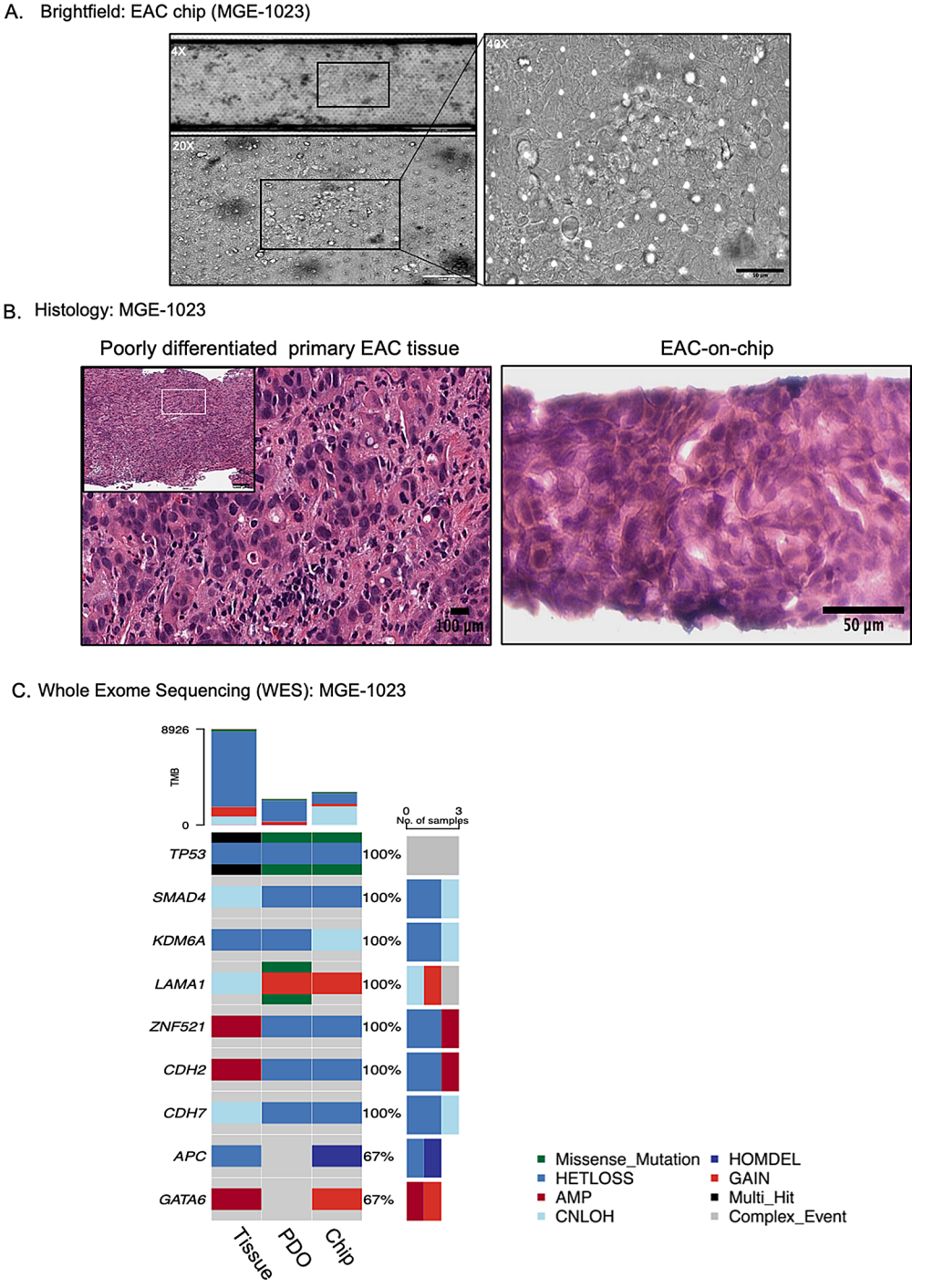

Fig. 4 EAC chips recapitulate the histology and genetic features of the source patient tissue. **(A)** Representative brightfield image of a horizontal section of the EAC-Chip derived from patient **MGE-1023**. **(B)** Representative H&E-stained image of an OCT®-embedded cryosection (30 µm) of on-chip EAC epithelium of **MGE-1023** (right) demonstrating histological similarity to a matched primary tumor section (5 µm, left). **(C)** Genetic materials from EAC patient (**MGE-1023)** on-a-chip recapitulates the genetic landscapes of primary tissues despite undergoing in vitro culture for several generations

effluents. According to the RECIST 1.1 criteria (objective responses), selected SENS patients ($n = 3$) experienced a reduction in tumor burden of more than 50% from baseline CT scans (Fig. 6). The decrease in CK19 fragment concentration in each treated chip effluent correlates with inpatient (source patient of the chip) chemotherapy-induced decrease in local tumor burden. SENS and RES chips both demonstrated a strong correlation with the corresponding objective responses to the regimen implemented for the chips (Fig. 6).

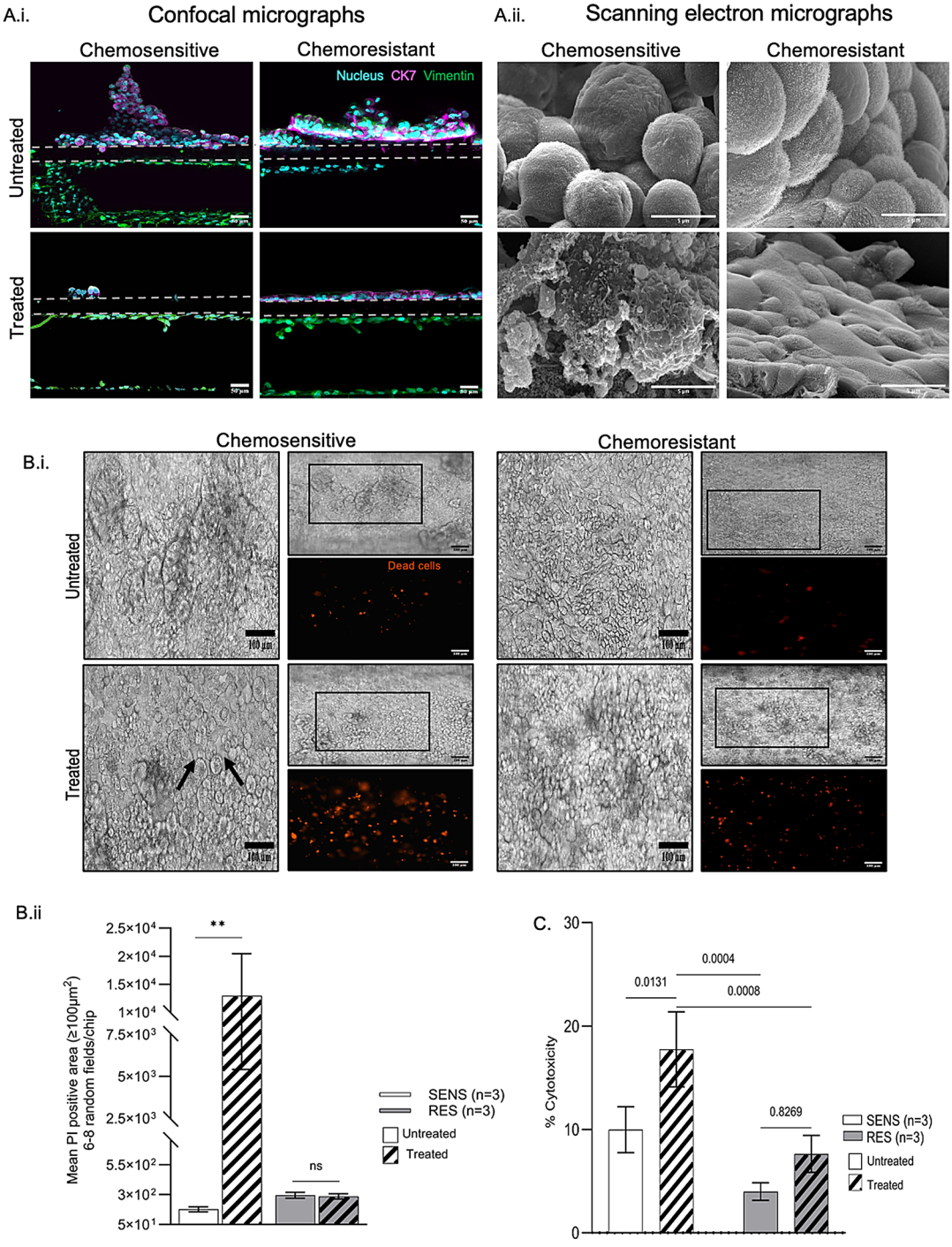

Fig. 5 Evaluation of clinical mimicry in EAC chips. EAC chips were subjected to 1 cycle (24 h) of FOT (Supplementary Table 2) at clinically relevant concentrations on day 8 *via* the stromal channel. The chips were maintained for another 72 h without chemotherapy. **(A) (i)** Representative confocal image showing near-complete eradication of epithelial cells ($CK7^+$) after 1 cycle of chemotherapy in the chemosensitive sample, whereas the epithelial layer remained intact in the chemoresistant sample. **(ii)** Representative SEM images demonstrating the disrupted surface of epithelial cell membranes in treated chemosensitive but not chemoresistant EAC-Chips. **(B) (i)** Representative live brightfield and fluorescence micrographs at 72 h posttreatment depict the different sensitivities of chemosensitive and chemoresistant samples. The black arrows indicate intercellular spaces affected by chemotherapy. **(ii)** The sizes of the dead (PI-positive; average cell area ≥ 100 μm2) regions in 6–8 random fields of intact chips were measured, and the sizes (mean ± SEM) are displayed as a bar graph, which shows larger affected area and additional dead cells in chemosensitive versus chemoresistant samples. *p* value **< 0.01, ns: not significant; Mann–Whitney U–Wilcoxon test. **(C)** EAC-chip effluents were collected on day 9 from the epithelial channel to determine LDH levels. The data revealed significantly greater LDH release in the chemosensitive samples than in the chemoresistant samples, indicating greater chemotherapy-mediated cytotoxicity. The data are presented as the mean percentage of cytotoxicity ± SEM. *p* values < 0.05; 2-way ANOVA

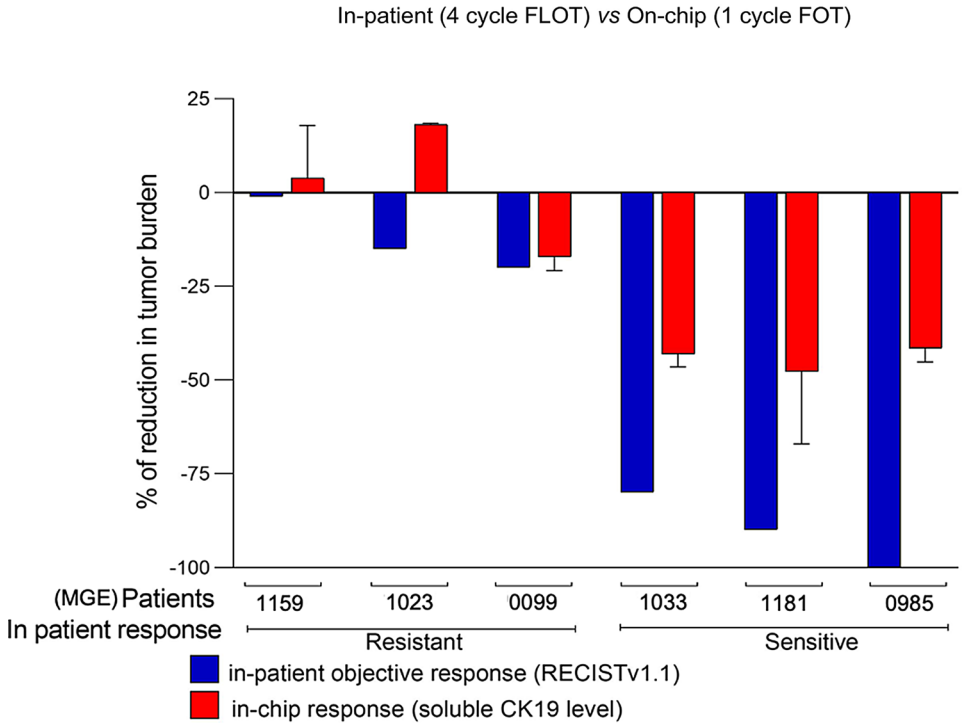

Fig. 6 The FOT regimen as reconstituted on EAC chips is highly effective with respect to the clinical response (RECIST v1.1). The merged comparative bar graph depicts matched inpatient objective responses to NACT (4 cycles) and in-chip NACT responses (1 cycle). All SENS patients had a > 50% reduction in tumor burden from baseline CT according to RECIST 1.1. Chip effluents were collected on day 11 (48 h after chemotherapy) for the CK19 fragment assay. The alterations in soluble CK19 fragment concentrations within EAC chip effluents before and after triplet chemotherapy are expressed as the mean percentage reduction in CK19 concentration ± SEM. This reduction is calculated separately by comparing the treated EAC-chips to their untreated counterparts

Discussion

Emerging evidence has indicated that the high degree of chemoresistance in locally advanced EAC is driven by both tumor and stromal heterogeneity. Developing accurate experimental models for EAC remains critically important due to the high morbidity and mortality linked to this aggressive esophageal cancer subtype. Currently, there are no spontaneously developing animal models for EAC. The most commonly used mouse model for EAC was developed by overexpressing interleukin-1β (IL-1β) in the esophagus and forestomach, which induces chronic inflammation, Barrett's esophagus-like metaplasia, and eventually EAC [50]. However, this process requires over 3–4 months, yields inconsistent results, as not all mice develop the full spectrum of disease, particularly EAC. While these models replicate certain features of human disease, the keratinized nature of the murine esophagus limits their utility for accurately assessing drug efficacy and toxicity. Patient-derived orthotopic xenograft (PDOX) models are occasionally employed to study EAC. Therefore, the novel model presented in this manuscript holds significant promise for advancing research in the EAC field.

Recently, significant advances have been made using patient-derived 3D tumor organoid-based culture systems, as this model faithfully preserves the heterogeneity of primary tumors and replicates patient responses to therapy. While PDOs offer more complex cellular structures than traditional cell cultures do, control over the microenvironment is not as precise as in organ-on-a-chip systems [32, 51–54]. Here, we highlighted potential shortcomings in the clinical relevance of static EAC-PDO monocultures when exposed to a combination of chemotherapeutics (only SOC available for locally advanced EAC patients). Standard organoid culture methods, in which PDOs are embedded in fragile Matrigel domes, do not allow for the precise recapitulation of the chemotherapy regimen the patient tumors experience in terms of dosing and timing of delivery. Consequently, chemotherapeutic agents continuously remain in the media for 24–72 h, often leading to bystander cytotoxicity, inconclusive IC_{50} or AUC values for determining chemoresistance. Notably, a few PDOs failed to respond consistently to clinically relevant triplet chemotherapeutic dose regimen, under static conditions. Standard organoid cultures allow for the assessment of resistance to monotherapies like oxaliplatin or 5-FU; however, they fall short in reliably replicating resistance to docetaxel, whether used alone or in combination with other drugs. Docetaxel is pharmacokinetically stable and highly toxic, which is why

patients typically receive it for only an hour. No human trials have been conducted in which patients received docetaxel for a duration longer than this. Therefore, our findings have aligned with previous clinical studies and indicated that static co-culture methods are not always suitable for such complex investigations. To overcome this issue, we reconstituted the clinical regimen of triplet chemotherapy ex vivo using this novel model. Furthermore, we also illustrated the advantages of integrating both PDO and microfluidic organ chip methodologies to generate a novel patient-specific preclinical EAC platform.

Patient specificity, fidelity, quality, functionality, and clinical significance comprise key parameters that we have addressed through the development of this platform. Although very few efforts have been made to create EAC-on-a-chip or 3D-EAC-bioprinted models [25], no patient-centered, physiologically, and clinically relevant EAC-chip system capable of emulating patients' innate response to chemotherapy is currently available. This platform is an excellent EAC organoid-based readout for assessing disease activity and treatment response.

For the first time, we have directly compared the in vivo response to a clinically relevant combinations of chemotherapeutics with in vitro models, including 2.5D, 3D tumor PDOs and organ chips. Our results demonstrate the superiority of the EAC-Chip in accurately replicating patient response. In accordance with our protocol (Fig. 1), PDOs and corresponding EAC chips can be developed within 5–6 weeks of a diagnostic biopsy, allowing for chemotherapy response prediction within the NACT timeline (approx. 2–3 months). These rapid results have the potential to offer alternative or salvage therapy options for chemoresistant patients at adjuvant time frames. This EAC-chip enables drug diffusion through the tumor-stroma interface, aiding in the study of differential cellular responses and the effects on tissue integrity and drug PK/PD. Since the current organ-chip system remains a low-throughput model, a static, 3D-PDO model is still required for HTP drug screening. Drugs demonstrating efficacy in the HTP screening can subsequently be evaluated using this high-fidelity, microfluidic organ-chip platform for more accurate prediction. This platform is also perfectly aligned with the guiding principles for ethical use of animals in research or 3Rs (Replacement, Reduction and Refinement).

Conclusions

This patient-specific EAC-Chip model can serve as a basis for the development of a functional precision oncology platform for this aggressive malignancy. However, this concept of implementing patient-specific tumors-on-a-chip is not limited to EAC; it can also be extended to various other cancer types.

Supplementary Information

The online version contains supplementary material available at https://doi.org/10.1186/s12967-025-06593-1.

Supplementary Material 1

Supplementary Material 2

Supplementary Material 3

Acknowledgements

LF and DI contributed equally to the study. We would like to thank the study participants who kindly permitted us to collect and use their biological material and clinical data. Schematic diagrams were prepared using BioRender. We also acknowledge the RI-MUHC BioBank platform for their role in obtaining patient consent and sample collection, the MUHC Pathology department for determining tumor content in primary tissue (Dr. Pierre-Olivier Fiset), Genome Quebec for their role in acquiring the whole exome sequencing data. Additionally, we would like to extend our acknowledgements for their technical assistance to the Histopathology and Molecular Imaging platforms at the Research Institute of the McGill University Health Centre, as well as to the Histology platform of the Goodman Cancer Institute at McGill University.

Author contributions

Conceptualization: SP, LF, and DI. Methodology: SP, ES, VS. Experiments: SP, MK, SFT, SDB, JB, KT. Visualization: SP. Funding acquisition: LF, VS. Project administration: NB. Supervision: LF, VS. Writing– original draft: SP. Writing–review & editing: SP, LF, DI, NB.

Funding

Montreal General Hospital Foundation (LF). Impact Grant award from the Department of Defense-Congressionally Directed Medical Research Programs, Award # CA200572 (LF, VS). STrOmal ReprograMing (STORMing Cancer); Cancer Research UK Grand Challenge.

Data availability

The primary data supporting the findings in this study are available within the manuscript and its Supplementary Information. The raw source and analysed datasets generated during the study are available for research purposes from the corresponding authors on reasonable request.

Declarations

Ethics approval and consent to participate

Patient data were used in this study, with informed consent obtained from each patient prior to the diagnostic biopsy. The study was approved by the Research Ethics Board of the McGill University Health Centre (protocols 2007 – 856 and 2021–7681).

Consent for publication

The study includes data from individuals who provided consent for their information without identity to be used exclusively for research purposes.

Conflict of interest

Dr. Donald E. Ingber is a founder, board member, and chairs the SAB of Emulate Inc., and holds equity. The remaining authors disclose no conflicts.

Author details

[1]Cancer Research Program, Research Institute of the McGill University Health Centre, Montreal, QC, Canada
[2]Wyss Institute for Biologically Inspired Engineering, Harvard University, Boston, USA
[3]Department of Bioengineering, McGill University, Montreal, Canada
[4]Department of Surgical and Interventional Sciences, McGill University, Montreal, Canada

Received: 12 February 2025 / Accepted: 8 May 2025
Published online: 23 May 2025

References

1. Morgan E, Soerjomataram I, Rumgay H, Coleman HG, Thrift AP, Vignat J, Laversanne M, Ferlay J, Arnold M. The global landscape of esophageal squamous cell carcinoma and esophageal adenocarcinoma incidence and mortality in 2020 and projections to 2040: new estimates from GLOBOCAN 2020. Gastroenterology. 2022;163(3):649–58. https://doi.org/10.1053/j.gastro.2022.05.054.
2. Ajani JA, D'Amico TA, Bentrem DJ, Cooke D, Corvera C, Das P, Enzinger PC, Enzler T, Farjah F, Gerdes H, et al. Esophageal and esophagogastric junction cancers, version 2.2023, NCCN clinical practice guidelines in oncology. J Natl Compr Canc Netw. 2023;21(4):393–422. https://doi.org/10.6004/jnccn.2023.0019.
3. Derouet MF, Allen J, Wilson GW, Ng C, Radulovich N, Kalimuthu S, Tsao MS, Darling GE, Yeung JC. Towards personalized induction therapy for esophageal adenocarcinoma: organoids derived from endoscopic biopsy recapitulate the pre-treatment tumor. Sci Rep. 2020;10(1):14514. https://doi.org/10.1038/s41598-020-71589-4.
4. Karakasheva TA, Gabre JT, Sachdeva UM, Cruz-Acuna R, Lin EW, DeMarshall M, Falk GW, Ginsberg GG, Yang Z, Kim MM, et al. Patient-derived organoids as a platform for modeling a patient's response to chemoradiotherapy in esophageal cancer. Sci Rep. 2021;11(1):21304. https://doi.org/10.1038/s41598-021-00706-8.
5. Liu H, Wang X. Esophageal organoids: applications and future prospects. J Mol Med (Berl). 2023;101(8):931–45. https://doi.org/10.1007/s00109-023-02340-5.
6. Ma X, Wang Q, Li G, Li H, Xu S, Pang D. Cancer organoids: A platform in basic and translational research. Genes Dis. 2024;11(2):614–32. https://doi.org/10.1016/j.gendis.2023.02.052.
7. Deben C, De La Hoz EC, Compte ML, Van Schil P, Hendriks JMH, Lauwers P, Yogeswaran SK, Lardon F, Pauwels P, Van Laere S, et al. OrBITS: label-free and time-lapse monitoring of patient derived organoids for advanced drug screening. Cell Oncol (Dordr). 2023;46(2):299–314. https://doi.org/10.1007/s13402-022-00750-0.
8. Gunther C, Winner B, Neurath MF, Stappenbeck TS. Organoids in Gastrointestinal diseases: from experimental models to clinical translation. Gut. 2022;71(9):1892–908. https://doi.org/10.1136/gutjnl-2021-326560.
9. Kijima T, Nakagawa H, Shimonosono M, Chandramouleeswaran PM, Hara T, Sahu V, Kasagi Y, Kikuchi O, Tanaka K, Giroux V, et al. Three-Dimensional organoids reveal therapy resistance of esophageal and oropharyngeal squamous cell carcinoma cells. Cell Mol Gastroenterol Hepatol. 2019;7(1):73–91. https://doi.org/10.1016/j.jcmgh.2018.09.003.
10. Yi K, Park SH, Kim DU, Jeon DY, Lee HJ, Song GA, Jo HJ, Baek DH, Han JH, Lee BC. Patient-derived organoid model for predicting the chemoresponse in patients with colorectal Cancer. Vivo. 2023;37(4):1751–9. https://doi.org/10.21873/invivo.13263.
11. Harada K, Sakamoto N. Cancer organoid applications to investigate chemotherapy resistance. Front Mol Biosci. 2022. https://doi.org/10.3389/fmolb.2022.1067207.
12. Ooft SN, Weeber F, Dijkstra KK, McLean CM, Kaing S, van Werkhoven E, Schipper L, Hoes L, Vis DJ, van de Haar J, et al. Patient-derived organoids can predict response to chemotherapy in metastatic colorectal cancer patients. Sci Transl Med. 2019;11:513. https://doi.org/10.1126/scitranslmed.aay2574.
13. Zaman MH, Trapani LM, Sieminski AL, Mackellar D, Gong H, Kamm RD, Wells A, Lauffenburger DA, Matsudaira P. Migration of tumor cells in 3D matrices is governed by matrix stiffness along with cell-matrix adhesion and proteolysis. Proc Natl Acad Sci U S A. 2006;103(29):10889–94. https://doi.org/10.1073/pnas.0604460103.
14. Ma P, Chen Y, Lai X, Zheng J, Ye E, Loh XJ, Zhao Y, Parikh BH, Su X, You M, et al. The translational application of hydrogel for organoid technology: challenges and future perspectives. Macromol Biosci. 2021;21(10):e2100191. https://doi.org/10.1002/mabi.202100191.
15. LeSavage BL, Suhar RA, Broguiere N, Lutolf MP, Heilshorn SC. Next-generation cancer organoids. Nat Mater. 2022;21(2):143–59. https://doi.org/10.1038/s41563-021-01057-5.
16. Flores-Torres S, Dimitriou NM, Pardo LA, Kort-Mascort J, Pal S, Peza-Chavez O, Kuasne H, Berube J, Bertos N, Park M, et al. Bioprinted multicomponent hydrogel Co-culture Tumor-Immune model for assessing and simulating Tumor-Infiltrated lymphocyte migration and functional activation. ACS Appl Mater Interfaces. 2023;15(28):33250–62. https://doi.org/10.1021/acsami.3c02995.
17. Flores-Torres S, Jiang T, Kort-Mascort J, Yang Y, Peza-Chavez O, Pal S, Mainolfi A, Pardo LA, Ferri L, Bertos N, et al. Constructing 3D in vitro models of heterocellular solid tumors and stromal tissues using Extrusion-Based Bioprinting. ACS Biomater Sci Eng. 2023;9(2):542–61. https://doi.org/10.1021/acsbiomaterials.2c00998.
18. Cruz-Acuna R, Kariuki SW, Sugiura K, Karaiskos S, Plaster EM, Loebel C, Efe G, Karakasheva T, Gabre JT, Hu J, et al. Engineered hydrogel reveals contribution of matrix mechanics to esophageal adenocarcinoma and identifies matrix-activated therapeutic targets. J Clin Invest. 2023;133(23). https://doi.org/10.1172/jci168146.
19. Zhu J, Ji L, Chen Y, Li H, Huang M, Dai Z, Wang J, Xiang D, Fu G, Lei Z, et al. Organoids and organs-on-chips: insights into predicting the efficacy of systemic treatment in colorectal cancer. Cell Death Discov. 2023;9(1):72. https://doi.org/10.1038/s41420-023-01354-9.
20. Lee SH, Contreras Panta EW, Gibbs D, Won Y, Min J, Zhang C, Roland JT, Hong SH, Sohn Y, Krystofiak E, et al. Apposition of fibroblasts with metaplastic gastric cells promotes dysplastic transition. Gastroenterology. 2023;165(2):374–90. https://doi.org/10.1053/j.gastro.2023.04.038.
21. Busslinger GA, Lissendorp F, Franken IA, van Hillegersberg R, Ruurda JP, Clevers H, de Maat MFG. The potential and challenges of patient-derived organoids in guiding the multimodality treatment of upper Gastrointestinal malignancies. Open Biol. 2020;10(4):190274. https://doi.org/10.1098/rsob.190274.
22. Zhao Y, Mei S, Huang Y, Chen J, Zhang X, Zhang P. Integrative analysis Deciphers the heterogeneity of cancer-associated fibroblast and implications on clinical outcomes in ovarian cancers. Comput Struct Biotechnol J. 2022;20:6403–11. https://doi.org/10.1016/j.csbj.2022.11.025.
23. Dunbar KJ, Karakasheva TA, Tang Q, Efe G, Lin EW, Harris M, Sahu V, Sachdeva UM, Hu J, Klein-Szanto AJ, et al. Tumor-Derived CCL5 recruits Cancer-Associated fibroblasts and promotes tumor cell proliferation in esophageal squamous cell carcinoma. Mol Cancer Res. 2023;21(7):741–52. https://doi.org/10.1158/1541-7786.MCR-22-0872.
24. Zhang CJ, Meyer SR, O'Meara MJ, Huang S, Capeling MM, Ferrer-Torres D, Childs CJ, Spence JR, Fontana RJ, Sexton JZ. A human liver organoid screening platform for DILI risk prediction. J Hepatol. 2023;78(5):998–1006. https://doi.org/10.1016/j.jhep.2023.01.019.
25. Shimshoni EMGE, Milot ZD, Oh CY, Horvath V, Gould RA, Caruso JA, Chen-Tanyolac C, Gascard P, Sangwan V, Bérubé J, Bailey SD, Hall S, Stachler MD, Ferri L, Tlsty TD, Ingber DE. Epithelial-Stromal interactions in Barrett's esophagus modeled in human organ chips. Gastro Hep Adv. 2023;2(5):676–80. https://doi.org/10.1016/j.gastha.2023.03.009.
26. Ingber DE. Is it time for reviewer 3 to request human organ chip experiments instead of animal validation studies?? Adv Sci (Weinh). 2020;7(22):2002030. https://doi.org/10.1002/advs.202002030.
27. Ingber DE. Human organs-on-chips for disease modelling, drug development and personalized medicine. Nat Rev Genet. 2022;23(8):467–91. https://doi.org/10.1038/s41576-022-00466-9.
28. Jang KJ, Otieno MA, Ronxhi J, Lim HK, Ewart L, Kodella KR, Petropolis DB, Kulkarni G, Rubins JE, Conegliano D, et al. Reproducing human and cross-species drug toxicities using a Liver-Chip. Sci Transl Med. 2019;11:517. https://doi.org/10.1126/scitranslmed.aax5516.
29. Tagle DA. The NIH microphysiological systems program: developing in vitro tools for safety and efficacy in drug development. Curr Opin Pharmacol. 2019;48:146–54. https://doi.org/10.1016/j.coph.2019.09.007.
30. Ewart L, Apostolou A, Briggs SA, Carman CV, Chaff JT, Heng AR, Jadalannagari S, Janardhanan J, Jang KJ, Joshipura SR, et al. Performance assessment and economic analysis of a human Liver-Chip for predictive toxicology. Commun Med (Lond). 2022;2(1):154. https://doi.org/10.1038/s43856-022-00209-1.
31. Carvalho MR, Yan LP, Li B, Zhang CH, He YL, Reis RL, Oliveira JM. Gastrointestinal organs and organoids-on-a-chip: advances and translation into the clinics. Biofabrication. 2023;15(4). https://doi.org/10.1088/1758-5090/acf8fb.
32. Thakar RG, Fenton KN. Bioethical implications of organ-on-a-chip on modernizing drug development. Artif Organs. 2023;47(10):1553–8. https://doi.org/10.1111/aor.14620.
33. Dickson I. Multispecies liver-on-a-chip for improved drug toxicity testing. Nat Rev Gastroenterol Hepatol. 2020;17(1):4. https://doi.org/10.1038/s41575-019-0244-5.
34. Li H, Durbin R. Fast and accurate short read alignment with Burrows-Wheeler transform. Bioinformatics. 2009;25(14):1754–60. https://doi.org/10.1093/bioinformatics/btp324.
35. McKenna A, Hanna M, Banks E, Sivachenko A, Cibulskis K, Kernytsky A, Garimella K, Altshuler D, Gabriel S, Daly M, et al. The genome analysis toolkit: a mapreduce framework for analyzing next-generation DNA sequencing data. Genome Res. 2010;20(9):1297–303. https://doi.org/10.1101/gr.107524.110.

36. Cibulskis K, Lawrence MS, Carter SL, Sivachenko A, Jaffe D, Sougnez C, Gabriel S, Meyerson M, Lander ES, Getz G. Sensitive detection of somatic point mutations in impure and heterogeneous cancer samples. Nat Biotechnol. 2013;31(3):213–9. https://doi.org/10.1038/nbt.2514.
37. Wang K, Li M, Hakonarson H. ANNOVAR: functional annotation of genetic variants from high-throughput sequencing data. Nucleic Acids Res. 2010;38(16):e164. https://doi.org/10.1093/nar/gkq603.
38. Shen R, Seshan VE. FACETS: allele-specific copy number and clonal heterogeneity analysis tool for high-throughput DNA sequencing. Nucleic Acids Res. 2016;44(16):e131. https://doi.org/10.1093/nar/gkw520.
39. Khanna A, Larson DE, Srivatsan SN, Mosior M, Abbott TE, Kiwala S, Ley TJ, Duncavage EJ, Walter MJ, Walker JR et al. Bam-readcount - rapid generation of basepair-resolution sequence metrics. ArXiv 2021.https://doi.org/10.21105/joss.03722
40. Wensink GE, Elias SG, Mullenders J, Koopman M, Boj SF, Kranenburg OW, Roodhart JML. Patient-derived organoids as a predictive biomarker for treatment response in cancer patients. NPJ Precis Oncol. 2021;5(1):30. https://doi.org/10.1038/s41698-021-00168-1.
41. Cancer Genome Atlas, Research N, Weinstein JN, Collisson EA, Mills GB, Shaw KR, Ozenberger BA, Ellrott K, Shmulevich I, Sander C, Stuart JM. The Cancer genome atlas Pan-Cancer analysis project. Nat Genet. 2013;45(10):1113–20. https://doi.org/10.1038/ng.2764.
42. Secrier M, Li X, de Silva N, Eldridge MD, Contino G, Bornschein J, MacRae S, Grehan N, O'Donovan M, Miremadi A, et al. Mutational signatures in esophageal adenocarcinoma define etiologically distinct subgroups with therapeutic relevance. Nat Genet. 2016;48(10):1131–41. https://doi.org/10.1038/ng.3659.
43. Nones K, Waddell N, Wayte N, Patch AM, Bailey P, Newell F, Holmes O, Fink JL, Quinn MCJ, Tang YH, et al. Genomic catastrophes frequently arise in esophageal adenocarcinoma and drive tumorigenesis. Nat Commun. 2014;5:5224. https://doi.org/10.1038/ncomms6224.
44. Brockmann JG, St Nottberg H, Glodny B, Heinecke A, Senninger NJ. CYFRA 21–1 serum analysis in patients with esophageal cancer. Clin Cancer Res. 2000;6(11):4249–52.
45. Brockmann JG, St Nottberg H, Glodny B, Sprakel B, Senninger N. Analysis of serum CYFRA 21–1 concentrations in patients with esophageal cancer. Anticancer Res. 2000;20(6D):4899–904.
46. Chu LY, Wu FC, Fang WK, Hong CQ, Huang LS, Zou HY, Peng YH, Chen H, Xie JJ, Xu YW. Secreted proteins encoded by super enhancer-driven genes could be promising biomarkers for early detection of esophageal squamous cell carcinoma. Biomed J 2023;100662. https://doi.org/10.1016/j.bj.2023.100662
47. Yajima S, Suzuki T, Oshima Y, Shiratori F, Funahashi K, Kawai S, Nanki T, Muraoka S, Urita Y, Saida Y, et al. New assay system Elecsys Anti-p53 to detect serum Anti-p53 antibodies in esophageal Cancer patients and colorectal Cancer patients: Multi-institutional study. Ann Surg Oncol. 2021;28(7):4007–15. https://doi.org/10.1245/s10434-020-09342-4.
48. Zhang R, Tian W, Zhao H, Zhang Z, Wu J, Sun S, Liu H. Effect of neoadjuvant therapy on serum transforming growth factor-beta, squamous cell carcinoma associated antigen, and prognosis in patients with locally advanced esophageal cancer. Cell Mol Biol (Noisy-le-grand). 2023;69(5):112–8. https://doi.org/10.14715/cmb/2023.69.5.18.
49. Ishioka N, Suzuki T, Yajima S, Murakami K, Ohkura Y, Fukuda T, Yagi K, Okamura A, Hoshino I, Kunisaki C, et al. Prognostic impact of pretreatment serum CYFRA status in 1047 patients with esophageal squamous cell carcinoma who underwent radical resection: A Japan esophageal society promotion research. Ann Thorac Cardiovasc Surg. 2022;28(3):163–70. https://doi.org/10.5761/atcs.oa.21-00195.
50. Martinez-Uribe O, Becker TC, Garman KS. Promises and limitations of current models for Understanding Barrett's esophagus and esophageal adenocarcinoma. Cell Mol Gastroenterol Hepatol. 2024;17(6):1025–38. https://doi.org/10.1016/j.jcmgh.2024.01.017.
51. Kim S, Naziripour A, Prabhala P, Horvath V, Junaid A, Breault DT, Goyal G, Ingber DE. Direct therapeutic effect of sulfadoxine-pyrimethamine on nutritional deficiency-induced enteric dysfunction in a human intestine chip. EBioMedicine. 2023;99:104921. https://doi.org/10.1016/j.ebiom.2023.104921.
52. Aggarwal RN, Sravani A, Mallya AB, Lewis P. Organ-On-A-Chip: an emerging research platform. Organogenesis. 2023;19(1):2278236. https://doi.org/10.1080/15476278.2023.2278236.
53. Sharma A, Jin L, Wang X, Wang YT, Stresser DM. Developing an adult stem cell derived microphysiological intestinal system for predicting oral prodrug bioconversion and permeability in humans. Lab Chip. 2023. https://doi.org/10.1039/d3lc00843f.
54. Apostolou A, Panchakshari RA, Banerjee A, Manatakis DV, Paraskevopoulou MD, Luc R, Abu-Ali G, Dimitriou A, Lucchesi C, Kulkarni G, et al. A novel microphysiological Colon platform to Decipher mechanisms driving human intestinal permeability. Cell Mol Gastroenterol Hepatol. 2021;12(5):1719–41. https://doi.org/10.1016/j.jcmgh.2021.07.004.

Publisher's note